



# Synthesis and evaluation of nickel doped Co<sub>3</sub>O<sub>4</sub> produced through hydrothermal technique

Leydi Julieta Cardenas-Flechas <sup>a</sup> Angela Mercedes Raba <sup>b</sup> & Miryam Rincón-Joya <sup>c</sup>

<sup>a</sup> Departamento de Ingeniería Mecánica y Mecatrónica, Facultad de Ingeniería, Universidad Nacional de Colombia, Bogotá, Colombia.  
*ljcardenasf@unal.edu.co*

<sup>b</sup> Departamento de Física, Facultad de Ciencias, Universidad Francisco de Paula Santander, Cúcuta, Colombia. *amrabap@gmail.com*

<sup>c</sup> Departamento de Física, Facultad de Ciencias, Universidad Nacional de Colombia, Bogotá, Colombia. *mrinconj@unal.edu.co*

Received: January 3<sup>rd</sup>, 2020. Received in revised form: April 3<sup>rd</sup>, 2020. Accepted: April 15<sup>th</sup>, 2020

## Abstract

The synthesis of undoped cobalt oxide and cobalt oxide with 4%nickel doping is studied in samples obtained through hydrothermal technique. After the final heat treatment at 300°C, X-ray diffraction analysis indicated the formation of cobalt spinel oxide with a complete replacement of nickel in the lattice. An average crystallite size of ~42 nm and ~31nm was found, as well as a particle size of ~ 20 nm and ~30 nm for Co<sub>3</sub>O<sub>4</sub> and Co<sub>3-x</sub>Ni<sub>x</sub>O<sub>4</sub>, respectively. Structural parameters were established through Rietveld refinement with a good correspondence between the simulated and the experimental pattern with values of  $\chi^2 = 1.25$  and GOF = 0.90 for Co<sub>3</sub>O<sub>4</sub>. The energy band gap was found through UV-Vis spectroscopy in two different regions: Eg<sub>1</sub> and Eg<sub>2</sub> values vary between 1.54 and 2.04eV for samples doped with nickel. The SEM results indicated the formation of nanostructures with semi-cubic shape and irregular rods. Parameters such as crystal size, particle size, surface area, as well as morphology of the final product depend on doping.

**Keywords:** cobalt oxide; doping, nanostructures; structural parameters.

# Síntesis y evaluación de Co<sub>3</sub>O<sub>4</sub> dopado con níquel producido mediante la técnica hidrotermal

## Resumen

La síntesis de óxido de cobalto con dopaje de níquel al 4% se estudia en muestras obtenidas mediante técnica hidrotermal. Después del tratamiento térmico final a 300°C, el análisis de difracción de rayos X indicó la formación de óxido de cobalto espinela con una substitución completa de níquel en la red. Se encontró un tamaño promedio de cristalito de ~42 nm ~31 nm, así como un tamaño de partícula de ~20 nm y ~30 nm para Co<sub>3</sub>O<sub>4</sub> y Co<sub>3-x</sub>Ni<sub>x</sub>O<sub>4</sub>, respectivamente. Los parámetros estructurales se establecieron mediante refinamiento Rietveld con una buena correspondencia entre el patrón simulado y el experimental con valores de  $\chi^2 = 1.25$  y GOF = 0.90 para Co<sub>3</sub>O<sub>4</sub>. La brecha de banda de energía se encontró a través de espectroscopía UV-Vis en dos regiones diferentes, los valores Eg<sub>1</sub> y Eg<sub>2</sub> varían entre 1.54 y 2.04eV para muestras dopadas con níquel. Los resultados SEM indicaron la formación de nanoestructuras con forma semicubica y bastones irregulares. Parámetros tales como el tamaño del cristal, el tamaño de partícula, el área de superficie, así como la morfología del producto final dependen del dopaje.

**Palabras clave:** óxido de cobalto; dopaje; nanoestructuras; parámetros estructurales.

## 1. Introduction

Metal oxides such as iron, cobalt, copper and zinc are candidates for a variety of important technological applications in catalysis, solar energy conversion,

electronics, magnetic media storage, etc. [1]. Recently, nanomaterials based on such oxides have been developed for various applications. Among these nanomaterials, Co<sub>3</sub>O<sub>4</sub> cobalt oxide has several morphologies and advantages, such as biological compatibility, broadband, high stability and low

**How to cite:** Cardenas-Flechas, L.J, Raba, A.M. and Rincón-Joya, M, Synthesis and evaluation of nickel doped Co<sub>3</sub>O<sub>4</sub> produced through hydrothermal technique. DYNA, 87(213), pp. 184-191, April - June, 2020.

cost [2]. Due to its good reproducibility and selectivity, this material has also been explored in fields such as supercapacitors and electrochemical sensors [3-5].

It is known that the behavior of nanophase materials depends largely on the shapes and sizes of the particles, which are, therefore, key factors in their performance and final applications [6]. Different electrical, optical, magnetic and mechanical properties in semiconductors can be achieved with a controlled size of nanoparticles. Nanostructured porous materials also have applications such as gas sensors, catalysis, among others [7,8]. Transition metal oxides with various oxidation states are very promising candidates for the high capacitance of the next generation, including nickel oxide. Regarding nickel, it has shown a very high specific capacity, low cost, low toxicity and respect for the environment, but with a relatively low cyclic reversibility [9].

The synthesis of cobalt oxide compounds with adjustable physicochemical properties has become a research point, where doping with transition metals improves properties such as electrical behavior as well as optical absorption [10]. Specifically, doping of  $\text{Co}_3\text{O}_4$  with nickel has shown significant changes in the behavior of the material. Improvement in the catalytic activity for the oxidation of CO through hybrid matrices is found in the most recent works of nickel doped  $\text{Co}_3\text{O}_4$  [11]. Wang et al. [9] evaluated the performance of solar-powered steam as a possible candidate for solar photothermal conversion using  $\text{Co}_3\text{O}_4$  nanoforest / Ni foam. Li et al. [12] analyzed the ORR activity according to the influence of nickel doping content. Ouyang et al. [13] concluded the excellent capacitive performance of the composite material attributed to the improved charge transfer rate and ion diffusion path. Additionally, Ren et al. [14] indicated that doping with Ni in the spinel lattice of  $\text{Co}_3\text{O}_4$  improves reaction kinetics and promotes catalytic activity.

In the present research,  $\text{Co}_3\text{O}_4$  and  $\text{Co}_3\text{O}_4$  doped with 4% nickel were synthesized by the hydrothermal technique and then calcining them at 300°C. The products obtained will be characterized using different techniques, such as X-ray diffraction and subsequently Rietveld refinement analysis. Samples of  $\text{Co}_3\text{O}_4$  have a crystalline structure after final heat treatment, and secondary phases belonging to the precursors used in the synthesis. SEM was used to observe the particle size and band gap results were obtained by UV-Vis. The research seeks to establish a comparison between  $\text{Co}_3\text{O}_4$  and  $\text{Co}_{3-x}\text{Ni}_x\text{O}_4$   $x=0.04$  studying the effect of hydrothermal synthesis.

## 2. Materials and methodology

### 2.1. Preparation of $\text{Co}_3\text{O}_4$

The synthesis was performed following the procedure of Jin et al. [15]. Initially, cobalt acetate and distilled water were used in the synthesis, then, urea and ammonia were added with constant stirring. The solution was carried in an autoclave for 20 hours at a temperature of 180 °C. Finally, the sample was washed with distilled water twice and the powders obtained were calcined at 300 °C for 3h.

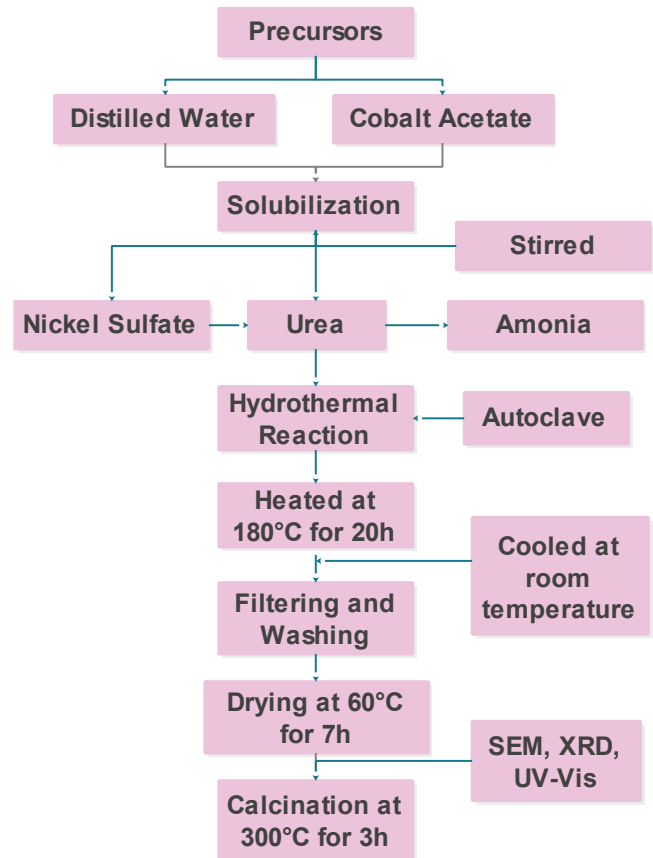


Figure 1. Schematic diagram of the hydrothermal process of  $\text{Co}_{3-x}\text{Ni}_x\text{O}_4$  preparation.  
Source: The Authors.

### 2.2. Preparation $\text{Co}_3\text{O}_4/\text{Ni}$ (4%)

Cobalt acetate was dissolved in distilled water. After solubilizing the components, nickel sulfate and, subsequently, urea were added. 2ml of ammonia were also added to adjust the pH. The solution was transferred to an autoclave and heated for 20 hours at 180°C. The samples obtained were washed with distilled water and ethanol and dried for 7 hours at 60°C. Finally, the powders were calcined at 300°C for 3 hours. Fig. 1 shows the schematic diagram of the hydrothermal process for the synthesis of nickel-doped  $\text{Co}_3\text{O}_4$ .

### 2.3. Characterization

The characterization of the samples was carried out using the techniques described below. The X-ray diffraction analysis (XRD) was performed on a PANalytical X'pert Pro equipment with data taken at an angle 2 between 100 and 800. It uses a RTMS (real time multiple strip) detector with  $\text{CuK}\alpha$  radiation, a wavelength of  $\lambda = 1.542\text{\AA}$  and a step of 0.02630 in Brentano Bragg mode, with subsequent Rietveld refinement of the experimental data, using the GSAS II code.

A Cary5000 UV-Vis-NIR diffractometer was used for measuring the UV-Vis reflectance spectrum in diffuse reflectance mode in the 200-2500 nm wavelength range.

With the aim to study the optical response of the  $\text{Co}_3\text{O}_4$ , the samples were measured with UV-visible electronic absorption spectroscopy. The morphological analysis was performed with a FEI Quanta 200 scanning electron microscope (SEM), in secondary electron mode at high vacuum and voltage of 30 KV. The qualitative chemical composition analysis was performed via energy dispersion microscopy (EDS).

### 3. Results and discussion

#### 3.1. Structural characterization

The spinel structure tolerates a high concentration of defects. This allows its physicochemical properties to be adjusted by doping and the insertion of several transition metals with various oxidation states at the spinel structure sites. The doping of  $\text{Co}_3\text{O}_4$  with nickel improves the electrical conductivity, which is related to the occupation of the doping site and its state of valence [16]. Fig. 2 shows the substitution of nickel at sites  $^{2+}$  and  $^{3+}$  of  $\text{Co}_3\text{O}_4$ . When nickel is added, it substitutes preferably the octahedral sites of  $\text{Co}^{3+}$  through stabilization at sites  $^{2+}$  and  $^{3+}$  [17]. According to Koneru et al. [18],  $\text{Ni}^{2+}$  at the tetrahedral sites leads to a normal spinel, while  $\text{Ni}^{2+}$  at the octahedral sites leads to an inverse spinel or a partial inverse spinel structure.

Fig. 3 shows the X-ray diffraction (XRD) pattern of  $\text{Co}_3\text{O}_4$  powder with the subsequent final heat treatment at 300°C for 3 hours and  $\text{Co}_3\text{O}_4$  doped with Ni and calcined during the same time. In section (a), the precursors obtained by the hydrothermal technique and examined by XRD are crystalline, though it is difficult to assign the definitive pattern to a specific phase. This condition has been present in other deposits [13]. In section (b),  $\text{Co}_3\text{O}_4$  was calcined at 300°C for 3h in air and the crystallinity of  $\text{Co}_3\text{O}_4$  is observed. In section (c), the pattern corresponds to the synthesis of  $\text{Co}_{3-x}\text{Ni}_x\text{O}_4$   $x=0.04$ , where the precursor peaks are observed again. Finally, in section (d), the pattern corresponds to  $\text{Co}_{3-x}\text{Ni}_x\text{O}_4$   $x=0.04$  after final heat treatment at 300°C-3h, where the intermediate peaks disappear completely and other diffraction peaks correspond to crystalline non-detected products. This indicates the high purity of the final heat treatment product.

All the powders obtained show diffraction peaks coinciding with the  $\text{Co}_3\text{O}_4$  cubic spinel structure (space group  $F-4 3m$ ) with file COD 00-001-1152. This agrees with other researches [13,19,20]. The XRD pattern with reflection peaks is associated with the planes (220), (311), (222), (400), (422), (511) and (440) at  $2\theta = 31.27^\circ$ ,  $36.88^\circ$ ,  $38.62^\circ$ ,  $44.81^\circ$ ,  $55.75^\circ$ ,  $59.45^\circ$  and  $65.38^\circ$ , respectively, and with the plane  $\langle 311 \rangle$  as preferential orientation. The  $2\theta$  position peaks observed in (a) and (c) at  $24.01^\circ$ ,  $32.69^\circ$ ,  $34.69^\circ$  are associated with the precursors used in the synthesis as  $(\text{Co}(\text{C}_2\text{H}_3\text{O}_2)_2 \cdot 4\text{H}_2\text{O}$  cobalt acetate. According to Singhal et al. [21], when the doping of nickel is carried out in  $\text{Co}_3\text{O}_4$ , a slight displacement is observed in the diffraction peaks.

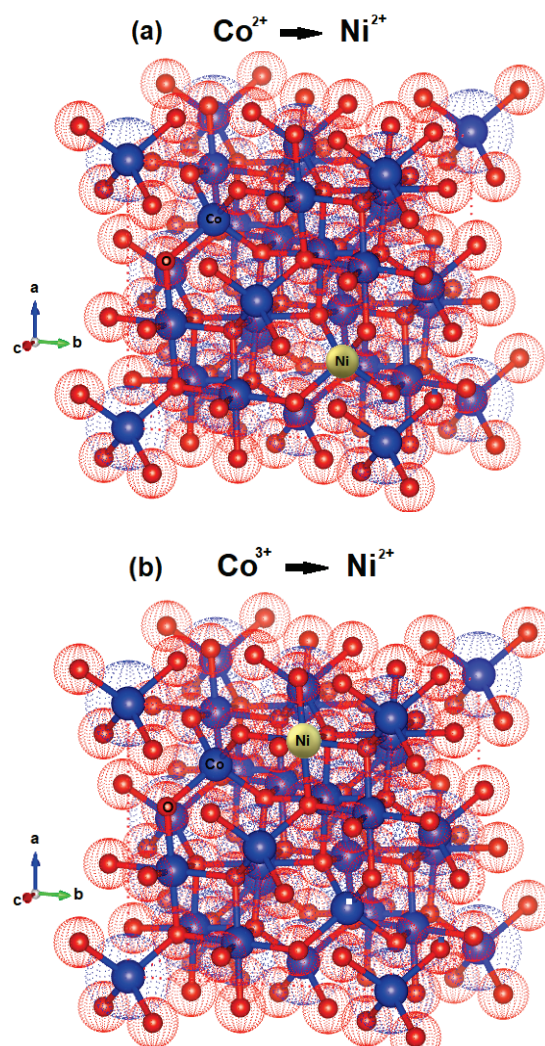


Figure 2. Bulk structure of spinel  $\text{Co}_3\text{O}_4$  with single tetragonal  $\text{Co}^{2+}$  cations (a) and single octahedral  $\text{Co}^{3+}$  (b), being replaced by  $\text{Ni}^{2+}$  cations.  
Source: The Authors using software Vesta.

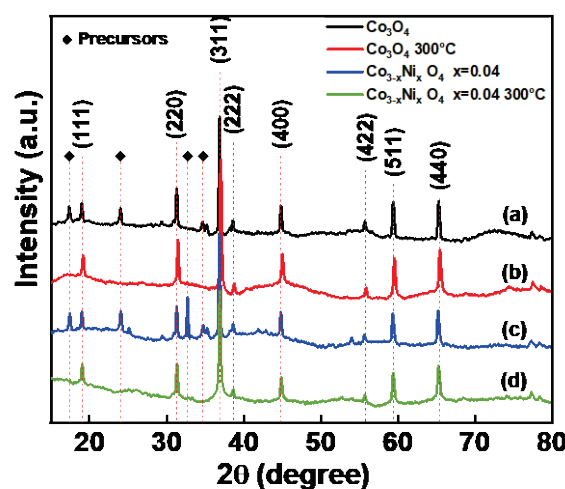


Figure 3. X-ray spectra (XRD) for the  $\text{Co}_3\text{O}_4$  samples obtained via hydrothermal technique: (a)  $\text{Co}_3\text{O}_4$ , (b)  $\text{Co}_3\text{O}_4$  300°C (c)  $\text{Co}_{3-x}\text{Ni}_x\text{O}_4$   $x=0.04$  and (d)  $\text{Co}_{3-x}\text{Ni}_x\text{O}_4$   $x=0.04$ -300°C.  
Source: The Authors.

Table 1.

Chemical composition of samples of  $\text{Co}_3\text{O}_4$  doped with nickel

$\text{Co}_3\text{O}_4$		$\text{Co}_3\text{O}_4-300^\circ\text{C}$		$\text{Co}_{3-x}\text{Ni}_x\text{O}_4$ $x=0.04$		$\text{Co}_{3-x}\text{Ni}_x\text{O}_4$ $x=0.04$ $300^\circ\text{C}$	
El.	% at	El.	% at	El.	% at	El.	% at
Co K	8.07	Co K	28.39	Co K	6.34	Co K	27.91
O K	44.08	O K	55.30	O K	56.97	O K	46.07
C K	8.07	C K	16.31	C K	36.37	C K	24.59
				Ni K	0.32	Ni K	1.43

Source: The Authors.

Table 1 shows the energy-dispersive spectrometry (EDS) analysis with the percentages of atomic concentration. Results indicate the presence of elements of  $\text{Co}_3\text{O}_4$  calcined at  $300^\circ\text{C}$ , as well as  $\text{Co}_3\text{O}_4$  doped with nickel and calcined. Elements such as Co, O, C and Ni appear according to the synthesis of each of the compounds.

In order to establish structural parameters and properties, Rietveld refinement was carried out with the experimental data using the GSASII code. Fig. 4 (a) corresponds to  $\text{Co}_3\text{O}_4$  and Fig. 4 (b) to  $\text{Co}_{3-x}\text{Ni}_x\text{O}_4$   $x=0.04$ -  $300^\circ\text{C}$ . The quality of the refinement can be checked through the values of the main refinement parameters:  $\chi^2=1.25$  and 1.26,  $R_{wp}=0.89\%$ , and 1.17% for  $\text{Co}_{3-x}\text{Ni}_x\text{O}_4$   $x=0.04$ - $300^\circ\text{C}$ . There is a good correspondence between the simulated and experimental pattern. Table 2 shows the lattice parameters of the refinement and in Table 3 the positions of  $\text{Co}_3\text{O}_4$  are observed. The refinement allowed to determine that  $\text{Co}_3\text{O}_4$  crystallizes in a spinel structure with a spatial group  $F-43m$  and with lattice parameters  $a=b=c=8.092630\text{\AA}$ . The refinement parameters are shown in Table 4, where values of GOF 0.90 and 1.13 are observed for  $\text{Co}_3\text{O}_4$  and  $\text{Co}_{3-x}\text{Ni}_x\text{O}_4$   $x=0.04$ - $300^\circ\text{C}$ , respectively. It has been observed that the lattice parameter and the unit cell volume for  $\text{Co}_3\text{O}_4$  are close to those found in the literature [22-24]. According to Mulinari et al. [25] the variation in the observed atomic positions in the oxygen atoms may be associated with the formation of distortions in the bonds [O-Co-O].

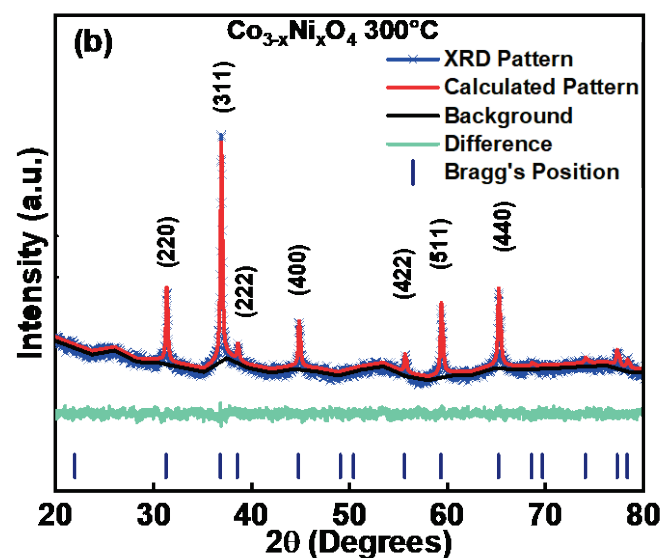
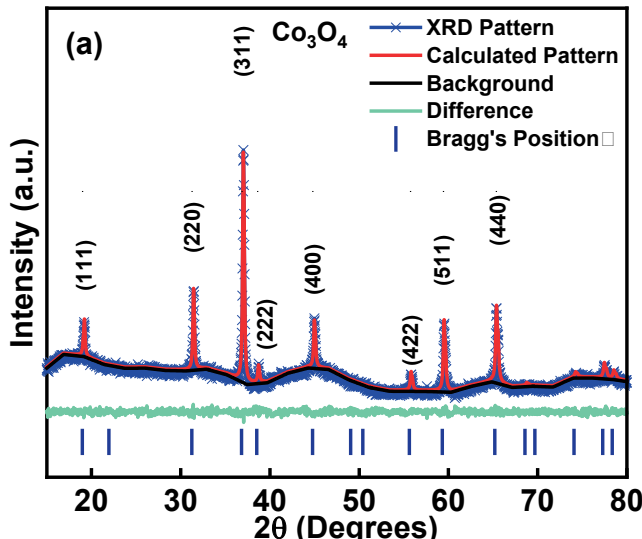


Figure 4 XRD refined pattern for the  $\text{Co}_3\text{O}_4$ - $300^\circ\text{C}$ . Blue symbols represent the experimental diffraction data. The continuous line is the calculated pattern and the difference between the experimental and calculated patterns is represented by the base line.

Source: The Authors.

Table 2.

Lattice parameters  $\text{Co}_3\text{O}_4$ 

$\text{Co}_3\text{O}_4$ Lattice Refinement parameters					
$a$ ( $\text{\AA}$ )	$b$ ( $\text{\AA}$ )	$c$ ( $\text{\AA}$ )	$\alpha$	$\beta$	$\gamma$
8.092630	8.092630	8.092630	90°C	90°C	90°C

Source: The Authors.

Table 3.

Positions  $\text{Co}_3\text{O}_4$ 

$\text{Co}_3\text{O}_4$ Positions		
	$x$	$y$
Co1	0.0000	0.0000
Co2	0.2500	0.2500
Co3	0.6250	0.6250
O1	0.3900	0.3900
O2	-0.1400	-0.1400

Source: The Authors.

Table 4.

Refinement parameters.

Refinement parameters $\text{Co}_3\text{O}_4$					
$\chi^2$	$R_{esp}$	$R_E$	$R(BS)$	$R_{wp}(BS)$	GOF
1.25	1.00%	0.71%	0.96%	0.89%	0.90
Refinement parameters $\text{Co}_{3-x}\text{Ni}_x\text{O}_4$ $x=0.04$ - $300^\circ\text{C}$					
$\chi^2$	$R_{esp}$	$R_E$	$R(BS)$	$R_{wp}(BS)$	GOF
1.26	1.04%	0.99%	1.23%	1.17%	1.13
Vol( $\text{\AA}^3$ )					
529.992					
529.854					

Source: The Authors.

### 3.2. Surface microstructure and composition

In Fig. 5, (a) and (c) indicate the SEM images of the precursors and (b) and (d) the products of  $\text{Co}_3\text{O}_4$  after final heat treatment. In (a), there are particles with semicircular forms, most of them well defined. In (b), agglomerations appear with certain rods in some of the particles. In (c), the

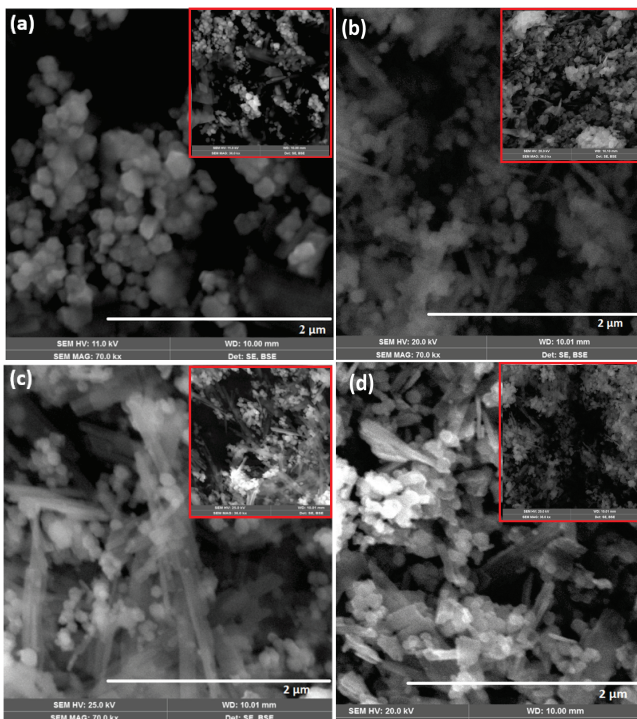


Figure. 5 SEM Images (a)  $\text{Co}_3\text{O}_4$  (b)  $\text{Co}_3\text{O}_4$  -300°C(c)  $\text{Co}_{3-x}\text{Ni}_x\text{O}_4$   
(d)  $\text{Co}_{3-x}\text{Ni}_x\text{O}_4$  -300°C.

Source: The Authors.

rods are notorious due to their diameter, and there are several particles. In (d), the structure is rather rough and has no definite shape. Irregular shapes are appreciated with agglomerations and certain inclusions that are attributed to nickel. The different forms obtained at 300 ° in (b) and (d) at 300°C are associated with the addition of nickel in the dopage in (d). Depending on the concentration of reagents,  $\text{Co}_3\text{O}_4$  nanoparticles with different shapes can be obtained [26].

It is assumed that temperature can affect surface morphology. According to Rajeshkhan et al. [27], different sizes of anions embedded in the reaction mixture are responsible for the formation of different morphologies during the growth of the cobalt oxide material. The preferential adsorption/desorption of anions in specific

crystallographic planes controls the formation of different morphologies, as well as the decrease in their surface energy.

Fig. 6 shows the process for synthesizing nickel-doped cobalt oxide. Initially, the mixture of nickel and cobalt is constantly stirred, with subsequent heating in the autoclave. Then, it was washed and dried.

As a result, nanostructures with semicubic and irregular rods were obtained. The autoclave was heated at 180°C for 20h (3°C/min), drying was carried out for 7h at 60 ° C in an oven, and the powders obtained were finally calcined in air at 300°C for 3h (10°C/min).

Organic and inorganic additives can be used to allow the precise control of various reaction parameters in the resulting composition, shape and size of nanocrystals, thanks to the liquid phase synthesis [28-30].

The average particle sizes were calculated by using the Debye Scherrer equation ( $0.9\lambda / (\beta \cos\theta)$ ) and obtaining the average crystallite size. The term  $\lambda$  is the wavelength, from full width to maximum half (FWHM) of the diffraction peak, and  $\theta$  is the Bragg Angle. The average particle size was calculated by using the most intense peak ( $\langle hkl \rangle$ ), (311). The crystallite size for  $\text{Co}_3\text{O}_4$  and  $\text{Co}_{3-x}\text{Ni}_x\text{O}_4$   $x=0.04$  was found at an average of 41.575nm with a slight decrease when nickel is added. For  $\text{Co}_3\text{O}_4$  at 300 ° C, the crystallite size decreases approximately 8 nm compared with  $\text{Co}_3\text{O}_4$  without final heat treatment and with a value of 33.85nm, and  $\text{Co}_{3-x}\text{Ni}_x\text{O}_4$   $x=0.04$  300°C at 12nm with a value of 29.89nm, as shown in Table 5. These results agree with the works of Singhal et al. [21,31] where the peaks represent a good crystallinity and they obtained a crystallite size of 36-42nm.

Table 5.  
Crystallite size calculation using the Debye Scherrer equation

Sample	Peak position (2θ)	FWHM (degree)	Crystallite size (nm)
$\text{Co}_3\text{O}_4$	36.85	0.1991	42.04
$\text{Co}_3\text{O}_4$ 300°C	37.03	0.2474	33.85
$\text{Co}_{3-x}\text{Ni}_x\text{O}_4$ $x=0.04$	36.87	0.2036	41.11
$\text{Co}_{3-x}\text{Ni}_x\text{O}_4$ $x=0.04$ 300°C	36.91	0.2801	29.89

Source: The Authors.

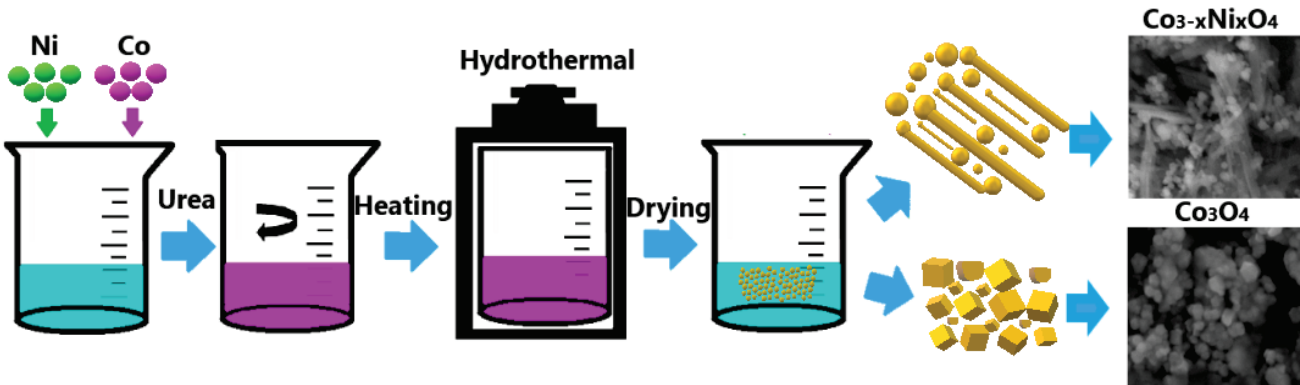


Figure. 6 Schematic illustration of the fabrication process of  $\text{Co}_3\text{O}_4$  -  $\text{Co}_{3-x}\text{Ni}_x\text{O}_4$ .  
Source: The Authors.

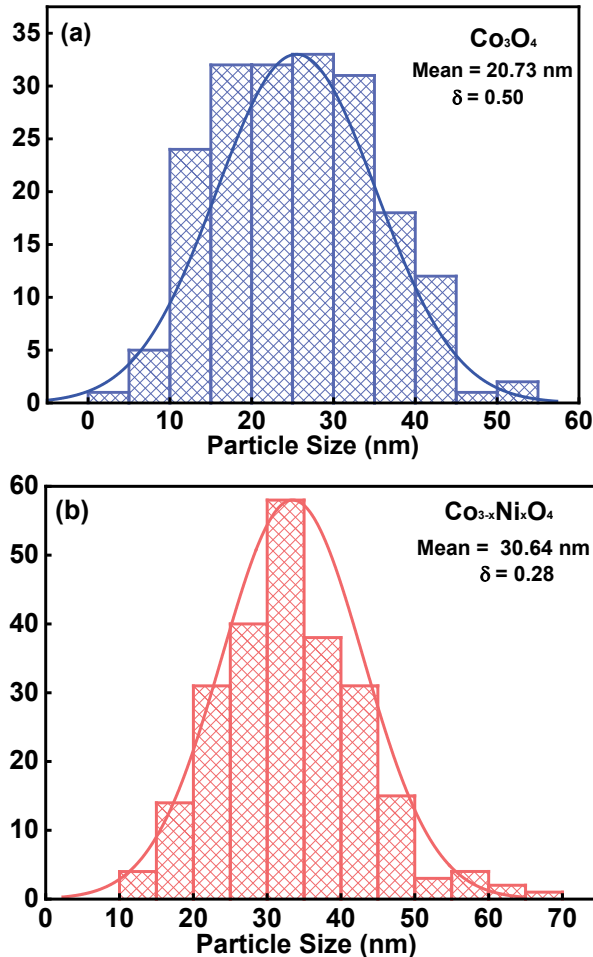


Figure 7. Particle Size: (a)  $\text{Co}_3\text{O}_4$  and (b)  $\text{Co}_{3-x}\text{Ni}_x\text{O}_4$   $x=0.04$   
Source: The Authors.

These results can also be associated with the research by Lakehal et al. [10], who prepared films and fine powders of nickel-doped cobalt oxide on glass substrates. They used an immersion coating process based on sol gel with a concentration of Ni in the range from 0 to 9% by weight (%). The crystallite size of the samples was in the range of 214-279 Å. According to Itteboina et al. [32], the heat treatment has an important role in particle size. Additionally, the crystallite size may be directly related to the nucleation table [33].

Fig. 7 shows the particle diameter size for (a)  $\text{Co}_3\text{O}_4$  that corresponds to 20.73 nm and (b)  $\text{Co}_{3-x}\text{Ni}_x\text{O}_4$  of 30.64 nm. This size increases when cobalt oxide is doped with nickel. The difference is approximately 9.91 nm. It has been found that nickel substitution improves cobalt-spinel oxide activity by enlarging its specific surface area, its conductivity and its roughness factor, which is also called electronic and geometric effect [34].

### 3.3. Optical band gap determination

Fig. 8 (a) shows the UV-Vis diffuse reflectance spectra of

$\text{Co}_3\text{O}_4$  alone and doped with 4% nickel, both calcined at 300°C. In the spectrum, the bandwidth values were calculated for the four samples shown in Table 6. The  $E_{g1}$  value found is  $E_{g1} = 1.51\text{eV}$  and correspond to  $\text{O}^{2-} \rightarrow \text{Co}^{3+}$  [35], while for  $E_{g2}$ , the value is  $E_{g2} = 2.74\text{eV}$ . For the  $\text{Co}_3\text{O}_4$  doped with 4% Ni, there is a slight increase in the band gap compared with pure  $\text{Co}_3\text{O}_4$ . The gap energy changed from 1.51 eV for pure  $\text{Co}_3\text{O}_4$  to 1.55 eV for the  $\text{Co}_3\text{O}_4$  doped with 4% Ni. For the calcined  $\text{Co}_3\text{O}_4$  doped with 4% Ni, there was also an increase compared with  $\text{Co}_3\text{O}_4$  at 300 °C (1.53 eV for  $\text{Co}_3\text{O}_4$  at 300°C and 1.56 eV for  $\text{Co}_3\text{O}_4$  at 300 °C with 4% Ni). The highest bandwidth energy changed from 2.74 eV for  $\text{Co}_3\text{O}_4$  to 1.54 eV for  $\text{Co}_3\text{O}_4$  at 300°C. This behavior can be attributed to the lattice distortions caused by the temperature change, as well as to the introduction of nickel ions in the  $\text{Co}_3\text{O}_4$  matrix and the formation of impurity energy levels (acceptor level) [10]. The morphology and structures of the materials are closely related to their optical properties, which are more evident in nanomaterials [36].

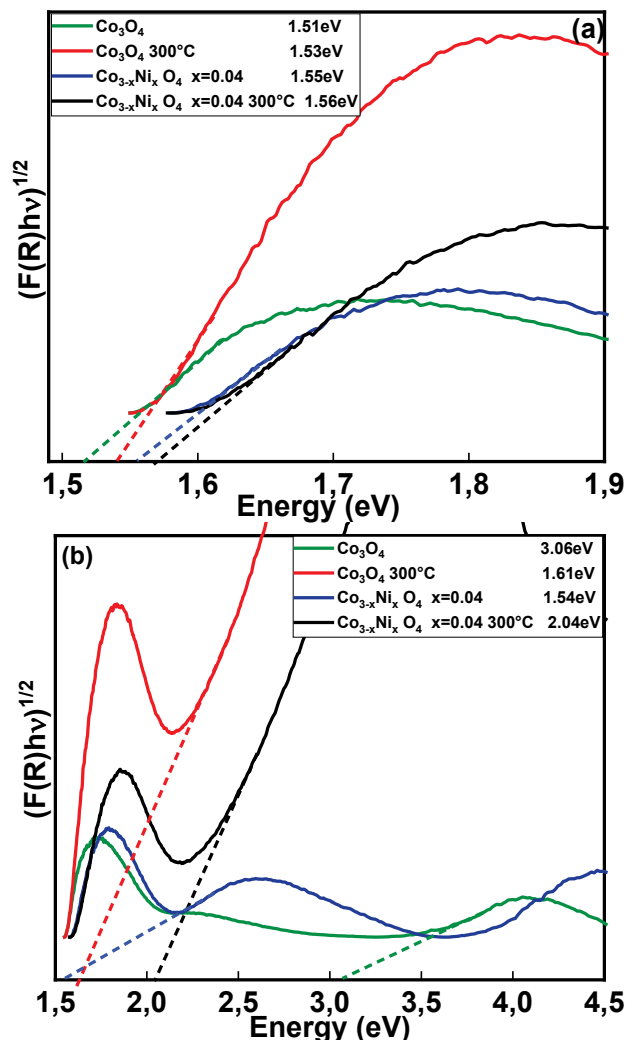


Figure 8. Determination of the band interval for  $\text{Co}_3\text{O}_4$ ,  $\text{Co}_3\text{O}_4$  at 300°C,  $\text{Co}_{3-x}\text{Ni}_x\text{O}_4$   $x=0.04$  and  $\text{Co}_{3-x}\text{Ni}_x\text{O}_4$   $x=0.04$  at 300°C for (a) the first region and (b) the second region.  
Source: The Authors.

Table 6.

Band Gap values for the first and second regions

Sample	Eg <sub>1</sub> (eV)	Eg <sub>2</sub> (eV)
Co <sub>3</sub> O <sub>4</sub>	1.51	2.74
Co <sub>3</sub> O <sub>4</sub> 300°C	1.53	1.61
Co <sub>3-x</sub> Ni <sub>x</sub> O <sub>4</sub> x=0.04	1.55	1.54
Co <sub>3-x</sub> Ni <sub>x</sub> O <sub>4</sub> x=0.04 300°C	1.56	2.04

Source: The Authors.

#### 4. Conclusions

Compounds of Co<sub>3</sub>O<sub>4</sub> and Co<sub>3-x</sub>Ni<sub>x</sub>O<sub>4</sub> with nickel doping were synthesized and the subsequent final heat treatment was performed at 300°C through the hydrothermal technique. After heat treatment, the results obtained indicated the crystallinity of Co<sub>3</sub>O<sub>4</sub> without the presence of Ni or NiO<sub>x</sub> impurities, according to the X-ray diffraction analysis. In the Co<sub>3-x</sub>Ni<sub>x</sub>O<sub>4</sub> compound, the heat treatment at 300°C allowed the conversion of the precursor to particles.

Structural characterization in samples of Co<sub>3</sub>O<sub>4</sub> and Co<sub>3-x</sub>Ni<sub>x</sub>O<sub>4</sub> was found through Rietveld refinement of experimental X-ray diffraction data. This evidenced that the samples initiate its major crystallization into a cubic structure belonging to the spatial group F-43m (# 216) with cell parameters a=b=c= 8.092630 Å with a slight variation in the volume value of the unit cell and a lower value for the nickel-doped compound of 529.584Å. The particle size varies between 20 and 30nm. Optical band gap measurements allowed to establish the value of Eg<sub>1</sub> and Eg<sub>2</sub> between 1.51 and 2.74eV for the samples of Co<sub>3</sub>O<sub>4</sub> calcinated and with doping.

#### References

- [1] Mahmood, S., Synthesis and characterizations of Co<sub>3</sub>O<sub>4</sub> based nanocomposite for electrochemical sensor applications. PhD Thesis, Faculty of Science, Malasya University, Malasya, 2018.
- [2] Ding, L., Zhao, M., Fan, S., Ma, Y., Liang, J., Wang, X. and Chen, S., Preparing Co<sub>3</sub>O<sub>4</sub> urchin-like hollow microspheres self-supporting architecture for improved glucose biosensing performance. Sensors and Actuators, B: Chemical, 235, pp. 162-169, 2016. DOI: 10.1016/j.snb.2016.05.068.
- [3] Hoa, L.T., Chung, J.S. and Hur, S.H., A highly sensitive enzyme-free glucose sensor based on Co<sub>3</sub>O<sub>4</sub> nanoflowers and 3D graphene oxide hydrogel fabricated via hydrothermal synthesis. Sensors and Actuators, B: Chemical, 223, pp. 76-82, 2016. DOI: 10.1016/j.snb.2015.09.009.
- [4] Dalkiran, B., Kaçar, C., Erden, P.E., and Kılıç, E., Amperometric xanthine biosensors based on chitosan- Co<sub>3</sub>O<sub>4</sub>- multiwall carbon nanotube modified glassy carbon electrode. Sensors and Actuators, B: Chemical, 2014, pp. 83-91, 2014. DOI: 10.1016/j.snb.2014.04.025.
- [5] Qing, X., Liu, S., Huang, K., Lv, K., Yang, Y., Lu, Z. and Liang, X., Facile synthesis of Co<sub>3</sub>O<sub>4</sub> nanoflowers grown on Ni foam with superior electrochemical performance. Electrochimica Acta, 56(14), pp. 4985-4991, 2011. DOI: 10.1016/j.electacta.2011.03.118.
- [6] Berenguer, R., Valdés-Solís, T., Fuertes, A.B., Quijada, C. and Morallón, E., Cyanide and phenol oxidation on nanostructured Co<sub>3</sub>O<sub>4</sub> electrodes prepared by different methods. Journal of the Electrochemical Society, 155(7), pp. 110-115, 2008. DOI: 10.1149/1.2917210.
- [7] Xiao, Y., Hu, C. and Cao, M., High lithium storage capacity and rate capability achieved by mesoporous Co<sub>3</sub>O<sub>4</sub> hierarchical nanobundles. Journal of Power Sources, 247, pp. 49-56, 2014. DOI: 10.1016/j.jpowsour.2013.08.069.
- [8] Liang, Y., Li, Y. and Wang, H., Co<sub>3</sub>O<sub>4</sub> nanocrystals on graphene as a synergistic catalyst for oxygen reduction reaction. Nature Mater, 10, pp. 780-786, 201. DOI:10.1038/nmat3087.
- [9] Wang, P., Gu, Y., Miao, L., Zhou, J., Su, H., Wei, A. and Cai, H., Co<sub>3</sub>O<sub>4</sub> nanoforest/Ni foam as the interface heating sheet for the efficient solar-driven water evaporation under one sun. Sustainable Materials and Technologies, 20, pp 1-7, 2019. DOI: 10.1016/j.susmat.2019.e00106.
- [10] Lakehal, A., Bedhiaf, B., Bouaza, A., Hadj, B., Ammari, A. and Dalache, C., Structural, optical and electrical properties of Ni-doped Co<sub>3</sub>O<sub>4</sub> prepared via Sol-Gel technique. Materials Research, 21(3), pp. 1-7, 2018. DOI: 10.1590/1980-5373-mr-2017-0545.
- [11] Mo, S., He, H., Ren, Q., Li, S., Zhang, W., Fu, M. and Ye, D., Macroporous Ni foam-supported Co<sub>3</sub>O<sub>4</sub> nanobrush and nanomace hybrid arrays for high-efficiency CO oxidation. Journal of Environmental Sciences, 75, pp. 136-144, 2019. DOI: 10.1016/j.jes.2018.02.026.
- [12] Li, S., Wu, K., Li, L., Suo, L. and Zhu, Y., An architecture of dandelion-type Ni- Co<sub>3</sub>O<sub>4</sub> microspheres on carbon nanotube films toward an efficient catalyst for oxygen reduction in zinc-air batteries. Applied Surface Science, 481, pp. 40-51, 2019. DOI: 10.1016/j.apsusc.2019.03.053.
- [13] Ouyang, K., Guo, G., Liu, Y., Sun, L. and Wei, M., Facile synthesis of heterogeneous Co<sub>3</sub>O<sub>4</sub>- nanowires/vertical-graphene-nanosheets on Ni foam for high performance supercapacitors. Materials Letters, 251, pp. 176-179, 2019. DOI: 10.1016/j.matlet.2019.05.062.
- [14] Ren, Z., Wu, Z., Song, W., Xiao, W., Guo, Y., Ding, J. and Gao, P.X., Low temperature propane oxidation over Co<sub>3</sub>O<sub>4</sub> based nano-array catalysts: Ni dopant effect, reaction mechanism and structural stability. Applied Catalysis B: Environmental, 180, pp. 150-160, 2016. DOI: 10.1016/j.apcatb.2015.04.021.
- [15] Jin, L., Li, X., Ming, H., Wang, H., Jia, Z., Fu, Y. and Zheng, J., Hydrothermal synthesis of Co<sub>3</sub>O<sub>4</sub> with different morphologies towards efficient Li-ion storage. RSC Advances, 4(12), pp. 6083-6089, 2014.
- [16] Bahlawane, N., Herve, P., Ngamou, T. and Kohse-höinghaus, K., Functional complex oxides: interplay between the structure, electrical properties and surface reactivity. Society, 516(c), pp. 3282-3282, 2009. DOI: 10.1039/C3RA45904G.
- [17] McClure, D.S., The distribution of transition metal cations in spinels. Journal of Physics and Chemistry of Solids, 3(3-4), pp. 311-317, 1957. DOI:10.1016/0022-3697(57)90034-3.
- [18] Koneru, A., Non-equilibrium Green's Function based calculations of spin voltage in cobalt based spinel oxides. PhD. Thesis, Department of Mechanical and Aerospace Engineering, West Virginia University, Virginia, United States, 2017.
- [19] Pan, A., Wang, Y., Xu, W., Nie, Z., Liang, S., Nie, Z. and Zhang, J.G., High-performance anode based on porous Co<sub>3</sub>O<sub>4</sub> nanodiscs. Journal of Power Sources, 255, pp. 125-129, 2014. DOI: 10.1016/j.jpowsour.2013.12.131.
- [20] Cao, J., Wang, S., Zhang, H. and Zhang, T., Constructing one dimensional Co<sub>3</sub>O<sub>4</sub> hierarchical nanofibers as efficient sensing materials for rapid acetone gas detection. Journal of Alloys and Compounds, 799, pp. 513-520, 2019. DOI: 10.1016/j.jallcom.2019.05.356.
- [21] Liang, M., Zhao, M., Wang, H., Wang, F. and Song, X., Excellent cycling stabilities of a novel calliandra-like Co<sub>3</sub>O<sub>4</sub> acted as anode materials for the lithium-ion battery. Journal of Energy Storage, 17, pp. 311-317, 2018. DOI: 10.1016/j.est.2018.03.017.
- [22] Singhal, A., Bisht, A. and Irusta, S., Enhanced oxygen evolution activity of Co<sub>3-x</sub>Ni<sub>x</sub>O<sub>4</sub> compared to Co<sub>3</sub>O<sub>4</sub> by low Ni doping. Journal of Electroanalytical Chemistry, 823, pp. 482-491, 2018. DOI: 10.1016/j.jelechem.2018.06.051.
- [23] Xiao, X., Liu, X., Zhao, H., Chen, D., Liu, F., Xiang, J. and Li, Y., Facile shape control of Co<sub>3</sub>O<sub>4</sub> and the effect of the crystal plane on electrochemical performance. Advanced materials, 24(42), pp. 5762-5766, 2012. DOI: 10.1002/adma.201202271.
- [24] Deng, S., Liu, X., Chen, N., Deng, D., Xiao, X. and Wang, Y., A highly sensitive VOC gas sensor using p-type mesoporous Co<sub>3</sub>O<sub>4</sub> nanosheets prepared by a facile chemical coprecipitation method. Sensors and Actuators B: Chemical, 233, pp. 615-623, 2016. DOI: 10.1016/j.snb.2016.04.138.

- [25] Mulinari, T.A., La Porta, F.A., Andrés, J., Cilense, M., Varela, J.A. and Longo, E., Microwave-hydrothermal synthesis of single-crystalline Co<sub>3</sub>O<sub>4</sub> spinel nanocubes. *CrystEngComm*, 15(37), pp. 7443-7449, 2013. DOI: 10.1039/C3CE41215F.
- [26] Li, L., Chu, Y., Liu, Y., Song, J., Wang, D. and Du, X., A facile hydrothermal route to synthesize novel Co<sub>3</sub>O<sub>4</sub> nanoplates. *Materials Letters*, 62(10-11), pp. 1507-1510, 2008. DOI: 10.1016/j.matlet.2007.09.012.
- [27] Rajeshkhan, G. and Ranga Rao, G., Micro and nano-architectures of Co<sub>3</sub>O<sub>4</sub> on Ni foam for electro-oxidation of methanol. *International Journal of Hydrogen Energy*, 43(9), pp. 4706-4715, 2018. DOI: 10.1016/j.ijhydene.2017.10.110.
- [28] Rajeshkhan, G., Umeshbabu, E. and Ranga Rao, G., Charge storage, electrocatalytic and sensing activities of nest-like nanostructured Co<sub>3</sub>O<sub>4</sub>. *Journal of Colloid and Interface Science*, 487, pp. 20-30, 2017. DOI: 10.1016/j.jcis.2016.10.011.
- [29] Umeshbabu, E., Rajeshkhan, G., Justin, P. and Rao, G.R., Magnetic, optical and electrocatalytic properties of urchin and sheaf-like NiCo<sub>2</sub>O<sub>4</sub> nanostructures. *Materials Chemistry and Physics*, 165, pp. 235-244, 2015. DOI: 10.1016/j.matchemphys.2015.09.023.
- [30] Meher, S.K. and Rao, G.R., Effect of microwave on the nanowire morphology, optical, magnetic, and pseudocapacitance behavior of Co<sub>3</sub>O<sub>4</sub>. *Journal of Physical Chemistry C*, 115(51), pp. 25543-25556, 2011. DOI: 10.1021/jp209165v.
- [31] Singhal, A., Bisht, A., Kumar, A. and Sharma, S., One pot, rapid synthesis of Co<sub>3</sub>O<sub>4</sub> by solution combustion method and its electrochemical properties in different electrolytes. *Journal of Electroanalytical Chemistry*, 776, pp. 152-161, 2016. DOI: 10.1016/j.jelechem.2016.07.004.
- [32] Itteboina, R. and Sau, T.K., Sol-gel synthesis and characterizations of morphology-controlled Co<sub>3</sub>O<sub>4</sub> particles. In: *Materials Today: Proceedings*, 9, 458-467, 2019. DOI: 10.1016/j.mtpr.2019.02.176.
- [33] Hu, Z., Oskam, G., Penn, R.L., Pesika, N. and Searson, P.C., The influence of anion on the coarsening kinetics of ZnO nanoparticles. *Journal of Physical Chemistry B*, 107(14), pp. 3124-3130, 2003. DOI: 10.1021/jp020580h.
- [34] Lu, B., Cao, D., Wang, P., Wang, G. and Gao, Y., Oxygen evolution reaction on Ni-substituted Co<sub>3</sub>O<sub>4</sub> nanowire array electrodes. *International Journal of Hydrogen Energy*, 36(1), pp. 72-78, 2010. DOI: 10.1016/j.ijhydene.2010.09.056.
- [35] Louardi, A., Rmili, A., Ouachtari, F., Bouaoud, A., Elidrissi, B. and Erguig, H., Characterization of cobalt oxide thin films prepared by a facile spray pyrolysis technique using perfume atomizer. *Journal of Alloys and Compounds*, 509(37), pp. 9183-9189, 2011. DOI: 10.1016/j.jallcom.2011.06.106.
- [36] Al-Tuwirqi, R., Al-Ghamdi, A.A., Aal, N.A., Umar, A. and Mahmoud, W.E., Facile synthesis and optical properties of Co<sub>3</sub>O<sub>4</sub> nanostructures by the microwave route. *Superlattices and Microstructures*, 49(4), pp. 416-421, 2011. DOI: 10.1016/j.spmi.2010.12.010.

**L.J. Cardenas-Flechas**, is BSc. Eng. in Electromechanical Engineering from the Universidad Pedagógica y Tecnológica de Colombia, Duitama, Boyacá in 2014. MSc. in Mechanical Engineering from at the Universidad Nacional de Colombia, Bogotá, Colombia. Currently, she is teaching assistant and PhD candidate in Engineering Materials Science and Technology at the Universidad Nacional Colombia, Bogotá. She has worked on thin films, corrosion resistance and synthesis by physical methods. ORCID: 0000-0001-6039-3924.

**A. Raba**, is MsC. in Physics from the Universidad Nacional de Colombia, Bogotá, Colombia. Currently, she is a PhD candidate in Physics at the Universidad Pedagógica y Tecnológica de Colombia and full professor and researcher at the Departamento de Física of the Universidad Francisco de Paula Santander, Colombia. ORCID: 0000-0001-8147-6323.

**M. Rincon-Joya**, is full professor at the Departamento de Física of the Universidad Nacional de Colombia, Bogotá Colombia. She conducts research in the general area of development and applications of synthesis by different techniques, analysis of optical properties etc. She received her PhD in 2008 from the Universidade Federal de São Carlos, Brasil. ORCID: 0000-0002-4130-9675



**UNIVERSIDAD NACIONAL DE COLOMBIA**

SEDE MEDELLÍN

FACULTAD DE MINAS

Área Curricular de Ingeniería  
Química e Ingeniería de Petróleos

Oferta de Posgrados

Doctorado en Ingeniería - Sistemas Energéticos  
Maestría en Ingeniería - Ingeniería Química  
Maestría en Ingeniería - Ingeniería de Petróleos

Mayor información:  
E-mail: qcaypet\_med@unal.edu.co  
Teléfono: (57-4) 425 5317